• Basic Research •

Human congenital cataract mutation in *MYH9* alters F-actin organization and cell functions

Hao Yuan[1,2], Zhen-Yu Wang[3], Jia-Rui Yang[1,2], Chen Huang[4], Liang Zhu[5], Xue-Min Li[1,2]

[1]Department of Ophthalmology, Peking University Third Hospital, Beijing 100191, China
[2]Beijing Key Laboratory of Restoration of Damaged Ocular Nerve, Beijing 100191, China
[3]Beijing Tongren Eye Center, Beijing Tongren Hospital, Beijing Ophthalmology and Visual Science Key Lab, Capital Medical University, Beijing 100191, China
[4]Medical Research Center, Peking University Third Hospital, Beijing 100191, China
[5]Wu Zuze Foundation for Sci-tech Development, Beijing 100191, China
Co-first Authors: Hao Yuan and Zhen-Yu Wang
Correspondence to: Liang Zhu. Wu Zuze Foundation for Sci-tech Development, Beijing 100191, China. 1206713511@qq.com. Xue-Min Li. Department of Ophthalmology, Peking University Third Hospital, Beijing 100191, China; Beijing Key Laboratory of Restoration of Damaged Ocular Nerve, Beijing 100191, China. lxmlxm66@sina.com.cn
Received: 2024-12-11 Accepted: 2025-03-11

Abstract

● **AIM:** To explore the role of a previously-found *MYH9* tail domain mutation (p.E1384Q) in the pathogenesis of congenital cataract.

● **METHODS:** The cell experiments were conducted *in vitro*. Wild-type (WT) *MYH9* and p.E1384Q mutant fragments were constructed, which was then transiently transfected into Hek293T cell lines. Western blotting and quantitative real time polymerase chain reaction (qRT-PCR) were used to analyze the protein and mRNA level of non-muscle myosin IIA (NM IIA) and F-actin in transfected cells, and fluorescence microscopy was applied to explore the subcellular localization of NM IIA and F-actin. Cell counting kit-8 (CCK8), wound-healing and double staining flow cytometry assays were performed to evaluate the proliferation, migration and apoptosis function of transfected cells, respectively. Transmission electron microscope was conducted to observe the alteration of organelle structure.

● **RESULTS:** The transiently-transfected WT and p.E1384Q mutant Hek293T cell lines was constructed. Western blot demonstrated that, comparing with $MYH9^{WT}$ group, the relative protein amount of NM IIA and F-actin significantly decreased in $MYH9^{E1384Q}$ cells ($P<0.001$). qRT-PCR analysis revealed that the relative mRNA amount of NM IIA and F-actin also significantly reduced in $MYH9^{E1384Q}$ cells when compared with $MYH9^{WT}$. The immunofluorescence microscopy showed that the fluorescence signal of NM IIA and F-actin significantly decreased in E1384Q cells. The diffuse cytoplasmic distribution of NM IIA in $MYH9^{WT}$ was changed to be clumped distribution, presenting a "speckled" pattern characterized by aggregates of small size in $MYH9^{E1384Q}$. Functional study revealed that the E1384Q mutation significantly inhibited cell proliferation ($P=0.003$) and migration ($P<0.001$), and promoted apoptosis ($P<0.001$). Electron microscope showed that the mutation remarkably decreased the number of mitochondria ($P<0.001$) and changed the phenotype of mitochondria.

● **CONCLUSION:** The missense gene mutation in *MYH9* (p.E1384Q) causing congenital cataract results in decreased amount and altered subcellular distribution of NM IIA and F-actin, accompanied by decreased cell proliferation and migration, promotes apoptosis and mitochondrial alteration.

● **KEYWORDS:** congenital cataract; *MYH9*; F-actin; cell function; mitochondria

DOI:10.18240/ijo.2025.06.01

Citation: Yuan H, Wang ZY, Yang JR, Huang C, Zhu L, Li XM. Human congenital cataract mutation in *MYH9* alters F-actin organization and cell functions. *Int J Ophthalmol* 2025;18(6):969-977

INTRODUCTION

Congenital cataract, a developmental anomaly characterized by opacities of the crystal lens that is present from birth, is the leading cause of restricted vision and blindness in children[1-5]. Although environmental factors are generally involved, about 8%–25% of isolated congenital cataracts are hereditary[6]. To date, over 50 identified genes have been linked with the pathogenesis of congenital cataracts, mainly of which encode structural protein crystallins, gap junctions, cytoskeletal proteins and DNA/RNA-binding proteins[7-11].

MYH9, a cytoskeletal gene encoding the heavy chain of non-muscle myosin of class II, isoform A (NM IIA), has recently been identified in the pathogenesis of congenital cataract[12]. Structurally, NM IIA is consisted of two anatomically distinct domains: the N-terminal head domain, which comprises the globular motor domain and the neck domain, and the C-terminal tail domain which is responsible for dimerization of the heavy chains and formation of NM IIA functional filaments[13-16]. Mammalian cells widely express three isoforms of class II non-muscle myosin (NM IIA, IIB, and IIC), which differ in their heavy chains, bind to F-actin cytoskeleton and produce mechanical force, participating in a variety of biological processes such as cytokinesis, cell migration, polarization, adhesion, maintenance of cell shape and signal transduction[17-19]. NM IIA and NM IIB are abundantly expressed in lens epithelial cells, which play crucial roles in embryonic development and morphological adjustment of lens[20].

In our previous research, we reported a three-generation Chinese family with 10 members, 4 of whom were diagnosed with autosomal dominant congenital cataract[21]. And by using target gene capture sequencing, we identified the pathological phenotype was resulted by a novel *MYH9* gene mutation (c.4150G>C, p.E1384Q) in the tail domain, leading to an amino acid substitution from glutamate to glutamine at codon 1384. According to the bioinformatics analysis, this mutation was predicted to be pathogenic. However, the detailed mechanism of *MYH9* mutation in the congenital cataract development is still unclear. Based on previous studies, the role of actin cytoskeletal organization in lens developmental has been extensively studied, including lens placode invagination, lens vesicle separation, epithelial morphogenesis, migration, differentiation and elongation into fiber cells[22]. Additionally, the role of NM IIA in mediating actin cytoskeleton assembling and polymerization has already been fully documented, and the mutation of *MYH9* could result in the disorganization of actomyosin cytoskeleton which interfered the microenvironment necessary for organ development[23-27]. Therefore, we speculated that E1384Q mutation in *MYH9* might affect the expression of NM IIA and disrupt the distribution of F-actin, thus potentially harming the biological functions of cells, which contributed to the onset of congenital cataract.

In this further study, we constructed wild-type (WT) *MYH9* and p.E1384Q mutant *MYH9* cell lines by transiently transfection methods. And we found the missense mutation consequently resulted in decreased amount and altered subcellular distribution of NM IIA and F-actin protein, accompanied by decreased cell proliferation and migration, promoted apoptosis and mitochondrial alteration.

METERIALS AND METHODS

Ethical Approval The study was designed as cell experiments *in vitro*, which was approved by the Ethics Committee of Peking University Third Hospital (approval number: M20241072) and adhered to the tenets of the Declaration of Helsinki.

Cell Culture and Gene Transfection The Hek293T cell line (YMbio Co., Beijing, China) was cultured in Dulbecco's modified Eagle's medium (DMEM) medium (Gibco, CA, USA) with 10% fetal bovine serum (Gibco, CA, USA) and 1% penicillin-streptomycin solution (Gibco, CA, USA) and supplemented at 37°C in the presence of 5% CO_2.

The full-length human WT *MYH9* (NM_002473.6) and mutant $MYH9^{E1384Q}$ fragments were synthesized by YMbio Co., Ltd. (Beijing, China). Both $MYH9^{WT}$ and $MYH9^{E1384Q}$ DNA sequences were firstly confirmed and inserted into pEGFP-N1 (CMV-MCS-EGFP-SV40-Neomycin; YouBio Co., Hunan, China), and then transformed into *Escherichia coli*. After classifying the positive clones by polymerase chain reaction (PCR) and DNA sequencing, Hek293T cells were cultured in 6-cm plates at a density of 5×10^5 cells/well and transfected with 4 μg of pEGFP-N1, pEGFP-N1-$MYH9^{WT}$ and pEGFP-N1-$MYH9^{E1384Q}$ plasmids DNA separately by Lipofectamine LTX (Invitrogen, CA, USA). The medium was renovated after 6h. After 48h, successfully transfected Hek293T cell lines were confirmed by fluorescence microscopy.

Western Blot and qRT-PCR Analysis The cell lysis buffer was utilized for harvesting and lysing the transfected cells. Total protein was collected and separated on 10% sodium dodecyl sulfate-polyacrylamide gel electrophoresis (SDS-PAGE) gels, then transferred to polyvinylidene difluoride (PVDF) membranes. The membranes were then blocked for 2h at room temperature with 5% non-fat milk, and incubated overnight at 4°C with primary antibodies against glyceraldehyde-3-phosphate dehydrogenase (GAPDH, 1:1000; Cat. #AB-P-R 001; Goodhere Biotech, Shanghai, China), NM IIA (1:1000; Cat. #ab138498; Abcam, Cambridge, UK) and F-actin (1:500; Cat. #ab130935; Abcam, Cambridge, UK). After 3-time washing (for 5min each) with Tris-buffered saline-Tween 20, the membranes were incubated with secondary antibody 1:600 HRP goat anti-rabbit IgG (Cat. #A0208; Beyotime Biotechnology, Shanghai, China), or 1:600 HRP goat anti-mouse IgG (Cat. #SA00001-1; Proteintech, Shanghai, China) for 2h at room temperature. Then they were washed for five times in Tris-Buffered saline with Tween-20 (TBST), followed by enhanced chemiluminescent detection to visualize the protein bands. Protein band intensities were quantified by Image J software [version 1.48v; National Institutes of Health (NIH), Bethesda, MD, USA; https://imagej.nih.gov/ij]. Values were normalized to GADPH loading control. All the results of

Western blots shown were representative of three independent experiments.

Trizol reagent (Invitrogen, Carlsbad, USA) was used to extract total RNA according to the manufacturer's protocol. After removing the genomic DNA with gDNA wiper Mix (Vazyme, Nanjing, China), cDNA was synthesized with reverse-transcription by HiScript II Select qRT SuperMix II (Vazyme, Nanjing, China). Then quantitative real time polymerase chain reaction (qRT-PCR) was performed using specific primers and SYBR Green Master Mix (Applied Biosystems, Foster City, USA) on an ABI QuantStudio 6 Flex qRT-PCR system (Applied Biosystems). The relative expression levels of NM IIA and F-actin mRNA to GADPH were obtained using threshold cycle values by $2^{-\triangle\triangle Ct}$ method.

Fluorescence Microscopy and Electron Microscope Transfected Hek293T cells were rinsed with phosphate-buffered saline (PBS) and fixed with 4% paraformaldehyde for 15min at room temperature. After incubation with TRITC-Phalloidin (Yeasen, Shanghai, China) for 1h followed by PBS washing; the nuclei were then labeled with 4,6-diamidino-2-phenylindole (Beyotime Biotech, Shanghai, China). Images were captured using Olympus (Tokyo, Japan) BX53 fluorescence microscope (1000× magnification), which were merged and labeled by Image J software. The staining process was repeated three times.

The pre-treated transfected cells were harvested and centrifuged by highspeed cryogenic centrifugation (1000 rpm) at 4°C for 5min and fixed in 2.5% glutaraldehyde (alfa Aesar; Thermo Fisher Scientific, Inc.) for 24h. After rinsing completely, the cells were incubated with osmium tetroxide and washed thoroughly. The cells were dehydrated using a graded series (30%, 50%, 70%, 80%, and 90%) of acetone solutions at 22°C to 25°C, then embedded in epoxy resin, followed by staining with uranyl acetate and lead citrate. Then, the subcellular structure was captured by the transmission electron microscope (HT7700-SS, Hitachi, Tokyo, Japan) at 3000, 5000 and 8000× magnification, respectively. To evaluate the number of mitochondria, 5 fields at 8000× magnification were randomly selected for each sample (3 samples per group) to count the overall number of intracellular mitochondria.

Cell Proliferation, Migration and Apoptosis The proliferative activity of transfected Hek293T cells was measured by the method of cell counting kit-8 (CCK-8). After being transfected by pEGFP-N1, pEGFP-N1-*MYH9*^{WT} and pEGFP-N1-*MYH9*^{E1384Q} plasmids, the cells were seeded into 96-well plates at a density of 5×10^3 cells/well and then cultured for 48h of incubation. Subsequently, 10 μL of CCK-8 (MedChemExpress, New Jersey, USA) was added to each well. After 2h of incubation at 37°C, a microplate reader (BioTek, Vermont, USA) was applied to assess the optical density values at 450 nm.

The wound-healing assay was performed to evaluate the migration function. The transfected Hek293T cells were seeded in 6-well plates at a density of 1.5×10^6 cells/well. When the cells grew to more than 90% confluency, a scratch wound was made by vertically scraping the cell cultures with a 200 μL micropipette tip. The cells were then washed with PBS to remove the debris and smooth the scratching edge. Images were captured using an Mshot (Guangzhou, China) MF52-N microscope at 0 and 24h after scraping (40× magnification). The relative migration area (difference between original wound area at 0 and new wound are at 24h) was measured with Image J software, and the cell migration rate was calculated as the ratio of relative migration area to original wound area.

The apoptosis status of transfected Hek293T cells was detected by double staining and then analyzed by flow cytometry. The Annexin V-APC/7-AAD Apoptosis Detection Kit (KeyGEN Biotech, Jiangsu, China) was applied. All the samples were analyzed using the flow cytometer (Beckman Coulter, CA, USA). All the above experiments were repeated three times.

Statistical Analysis Measurement values were presented as the means±standard deviations (SD) with at least three independent experiments. SPSS 23.0 (IBM, NY, USA) was applied to perform the statistical analyses. The distribution mode of data was assessed by Shapiro-Wilk normality test, and multiple intergroup comparisons were performed by one-way ANOVA with Bonferroni's post hoc tests. *P* value less than 0.05 would be considered statistically significant. No human participant's data, including tissue sample, was involved in our research, so informed consent was not needed.

RESULTS

Immunoblotting and qRT-PCR In Hek293T cells transfected with pEGFP-N1-*MYH9* plasmids, Western blots indicated that, compared with control and vector groups, the protein level of NM IIA was significantly increased in both *MYH9*^{WT} (Figure 1A, 1E; $P<0.001$) and *MYH9*^{E1384Q} groups (Figure 1A, 1E; $P<0.05$), revealing the successful transfection and expression of exogenous plasmids. Meanwhile, when compared with the WT group, E1384Q mutation significantly reduced the level of NM IIA protein (Figure 1A, 1E; $P=0.004$). Similarly, comparing with WT group, we also detected significantly reduced F-actin protein level in E1384Q mutation group (Figure 1B, 1E; $P<0.001$). qRT-PCR analysis was performed to demonstrate that the expression of *MYH9* (Figure 1C, 1E; $P<0.001$) was remarkably decreased in *MYH9*^{E1384Q} group comparing to *MYH9*^{WT} group, as well as the mRNA level of *F-actin* (Figure 1D, 1E; $P<0.001$).

Immunofluorescence Analysis The immunofluorescence microscopy showed that, when compared with *MYH9*^{WT} cells, green fluorescence signal, which indicated the existence of EGFP-NM IIA protein, was relatively weaker in cells

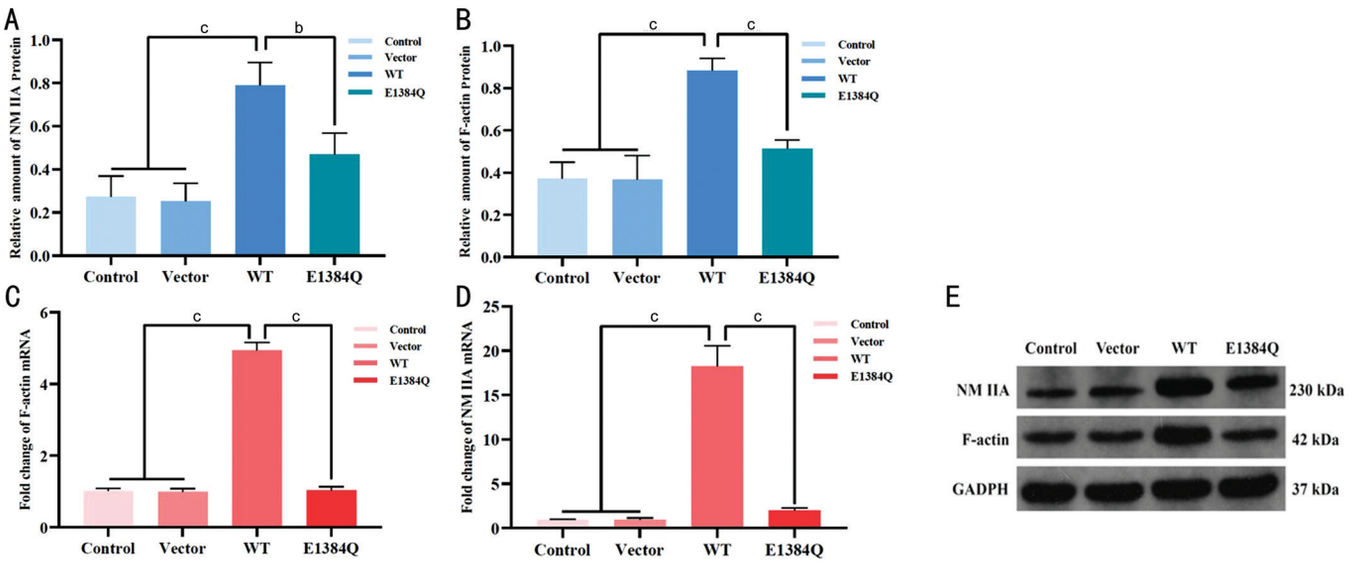

Figure 1 The protein and mRNA level of NM IIA and F-actin in transfected Hek293T cells A, B: Western blot demonstrated that, comparing with *MYH9*^{WT} group, the relative protein amount of NM IIA and F-actin significantly decreased in *MYH9*^{E1384Q} mutation Hek293T cells; C, D: RT-qPCR analysis revealed that the relative mRNA amount of NM IIA and F-actin significantly reduced in *MYH9*^{E1384Q} mutation Hek293T cells when compared with *MYH9*^{WT} group; E: The immunoblotting showed that, comparing with WT group, the *MYH9*^{E1384Q} mutation significantly reduced protein expression level of NM IIA and F-actin in transfected Hek293T cells. NM IIA: Non-muscle myosin of class II, isoform A; WT: Wild type; RT-qPCR: Quantitative real time polymerase chain reaction. $^{b}P<0.01$; $^{c}P<0.001$.

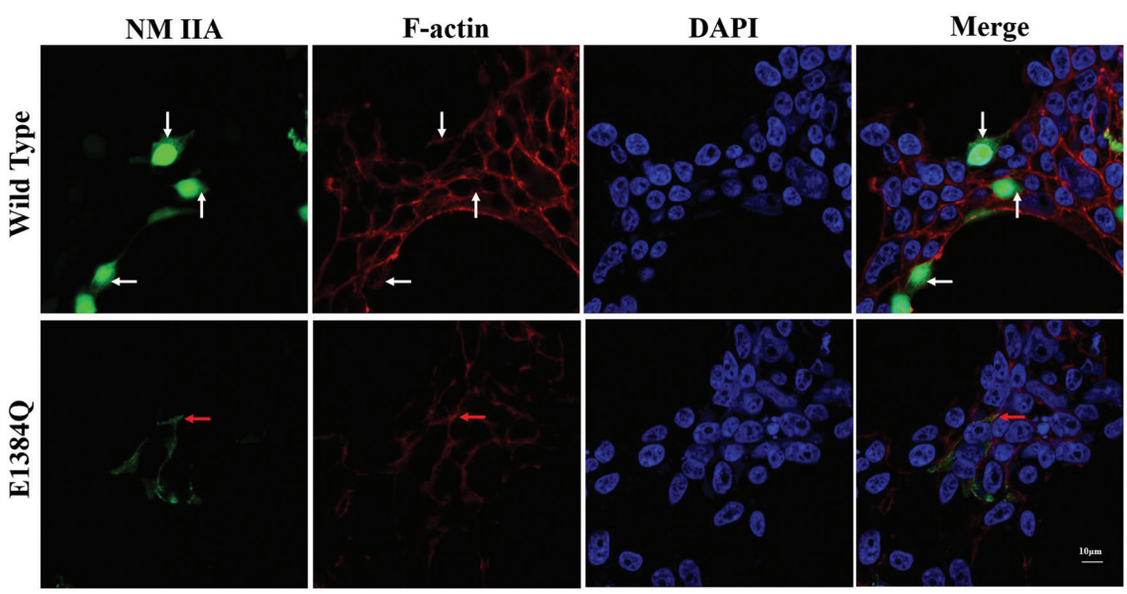

Figure 2 The colocalization of NM IIA (green fluorescence), F-actin (red fluorescence) and nuclei (blue fluorescence) in transient transfected Hek293T cells Scale bar: 10 μm; White arrows: The colocalization of NM IIA and F-actin in *MYH9*^{WT} cells; Red arrows: The colocalization of NM IIA and F-actin in *MYH9*^{E1384Q} cells. NM IIA: Non-muscle myosin of class II, isoform A; DAPI: 4,6-diamidino-2-phenylindole.

expressing E1384Q mutant protein (Figure 2). In *MYH9*^{WT} cells, NM IIA could be predominantly seen in cell cytoplasm with diffuse distribution (Figure 2). While in *MYH9*^{E1384Q} cells, we found that the green fluorescence in cytoplasm was obviously decreased, and NM IIA mostly showed clumped distribution, presenting a "speckled" pattern characterized by aggregates of small size (Figure 2).

Double labeling immunofluorescence experiment of NM IIA and F-actin in transfected cells was conducted. We detected that F-actin in *MYH9*^{WT} group showed distinct linear membrane expression, especially at the intercellular borders, and was companied by diffuse perimembranous and cytoplasmic distribution (Figure 2). In contrast, the pattern in *MYH9*^{E1384Q} cells was changed to be intermittent clumped membrane distribution, without noticeable intracellular staining (Figure 2). In *MYH9*^{WT} Hek293T cells, it was common to find the colocalizations of NM IIA with F-actin (Figure 2, white arrows), almost exclusively at cell boundary. In E1384Q

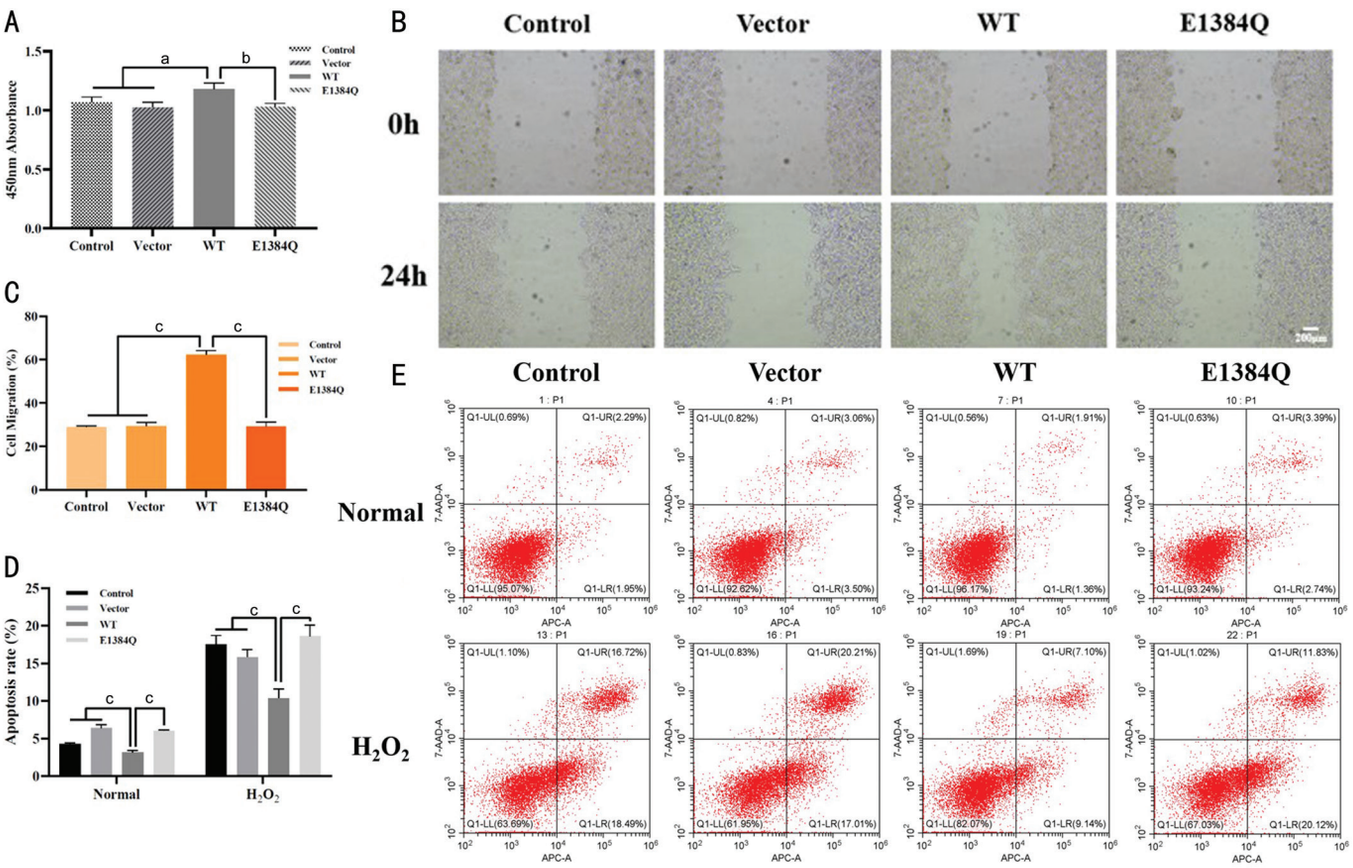

Figure 3 The proliferation, migration and apoptosis function of transient transfected Hek293T cells A: CCK8 assay demonstrated that 450 nm absorbance of transfected cells significantly reduced in *MYH9*^{E1384Q} group than WT group; B, C: Wound-healing assay showed that *MYH9*^{E1384Q} cells migrated significantly slower than WT cells after 24-hour observation. Scale bar: 200 μm. D, E: The apoptosis rate by double staining flow cytometry remarkably increased in *MYH9*^{E1384Q} cells compared with WT cells. WT: Wild type. $^{a}P<0.05$, $^{b}P<0.01$, $^{c}P<0.001$.

mutant group, NM IIA still showed some perimembranous colocalization with F-actin (Figure 2, red arrows), although not precisely colocalized. The green fluorescence signal (NM IIA) was sparsely distributed in the cytoplasm with little red fluorescence signal (F-actin, Figure 2).

Cell Function Cell proliferation function was evaluated by CCK8 assay. Comparing with both control (1.07±0.04) and vector (1.03±0.05) groups, *MYH9*^{WT} cells showed remarkably promoted proliferation function with 1.18±0.05 at 450 nm absorbance (Figure 3A; control group, P=0.013; vector group, P=0.002). The optical density in *MYH9*^{E1384Q} group was 1.03±0.03, appearing decreased cellular viability than WT group (P=0.003; Figure 3A) and no significant difference compared with both control (P=0.325) and vector (P=0.855) groups.

Wound-healing assay was then performed to assess cell migration. Compared with both control (28.86%±0.51% area) and vector (29.32%±1.72% area) groups, Hek293T cells transfected with *MYH9*^{WT} plasmid showed remarkably faster migration after 24h, occupying 62.27%±1.99% of the cell-free area after 24h (both P<0.001; Figure 3B, 3C). And cells expressing E1384Q mutant protein migrated significantly slower than WT group, with 29.09%±2.09% area occupied after 24h (both P<0.001; Figure 3B, 3C), but showing no significant difference compared with both control (P=0.873) and vector (P=0.872) groups.

Cell apoptosis was analyzed by AnnexinV-APC/7-AAD double staining flow cytometry. Comparing with both control (4.27%±0.15%) and vector (6.37%±0.43%) groups, apoptosis was significantly inhibited in *MYH9*^{WT} cells, with the total apoptosis rate of 3.16%±0.27% (Figure 3D, 3E; both P<0.001). However, cells transfected with *MYH9*^{E1384Q} plasmids showed a higher apoptosis proportion than WT group (P<0.001; Figure 3D, 3E).

Electron Microscope We performed transmission electron microscope to explore the alteration of subcellular structure and organelle distribution. Compared with *MYH9*^{E1384Q} group that mitochondria were sparsely dispersed, mitochondria in *MYH9*^{WT} cells were relatively more abundantly distributed (Figure 4A, 4D). The counted number of mitochondria in *MYH9*^{WT} group was 52.00±4.726, which was significantly higher than that in *MYH9*^{E1384Q} group (26.33±0.667, P<0.001). Moreover, mitochondria in *MYH9*^{WT} cells showed large volume, rod-like shape and compact crista (Figure 4B).

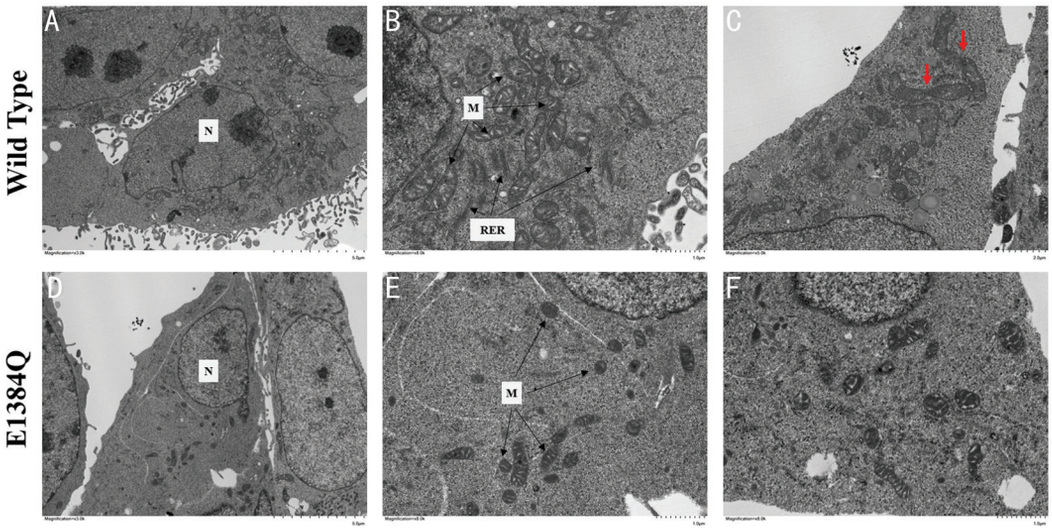

Figure 4 The transmission electron microscope observation in transient transfected Hek293T cells A: The mitochondria were abundantly distributed in *MYH9*^{WT} cells. Scale bar: 5.0 μm. B: The mitochondria in *MYH9*^{WT} cells showed large volume, rod-like shape and compact crista. Scale bar: 1.0 μm. C: The mitotic mitochondria were detected in *MYH9*^{WT} cells, indicating active mitochondrial division. Scale bar: 1.0 μm; Red arrows: Mitotic mitochondria. D: The mitochondria were sparsely distributed in *MYH9*^{E1384Q} cells. Scale bar: 5.0 μm. E: The mitochondria in *MYH9*^{E1384Q} cells showed small volume, round shape and thin crista. Scale bar: 1.0 μm. F: No mitotic mitochondria were detected in *MYH9*^{E1384Q} cells. Scale bar: 1.0 μm. N: Nucleus; M: Mitochondria; RER: Rough endoplasmic reticulum.

Instead, mitochondria in *MYH9*^{E1384Q} cells exhibited small volume, round shape and thin crista (Figure 4E). Additionally, we also detected several rough endoplasmic reticula and mitotic mitochondria in *MYH9*^{WT} group (Figure 4B, 4C), indicating active protein synthesis, vesicular transportation and energy metabolism, which were not prominently found in E1384Q mutant group (Figure 4F).

DISCUSSION

MYH9, a highly conserved gene, has increasingly been identified in the pathogenesis of congenital cataract. Previous studies have revealed that NM IIA is abundantly expressed in lens epithelial cells, and plays a crucial role in embryonic development and morphological adjustment of lens[20,28-29]. Therefore, the function of *MYH9* must be closely correlated with lens development and cataract onset.

To explore the potential mechanism of novel *MYH9* missense mutation in congenital cataract, the loss-of function of myosin IIA resulted from reduced E1384Q mutant protein level was first considered. Our results of Western blot and qRT-PCR consistently suggested a dramatical declined expression of mutant *MYH9* in both mRNA and protein level. Similarly, Vettore *et al*[30] reported a family with a novel identified *MYH9* mutation (p.R1162T) and detected decreased NM IIA protein level in their platelets compared with normal controls. Pecci *et al*[31] found that the mutant *MYH9* protein (R1933X) was not even significantly expressed in platelets and granulocytes isolated from patients' peripheral blood. Given that *MYH9* mRNA level was stable in majority of previous researches, it was traditionally accepted that the decreased protein content was caused by post-translational degradation[32]. However, our results suggested that mRNA level of *MYH9* was also reduced in *MYH9*^{E1384Q} cells, indicating that the post-transcriptional modification of mRNA should be investigated in further research.

By immunofluorescence analysis, we found the distribution of NM IIA was disrupted in mutant cells, which has been fully elaborated in *MYH9* mutations. Traditionally, myosin IIA is diffusely distributed throughout the cytoplasm in a uniform pattern[33]. However, in *MYH9*-RD patients, mutant myosin IIA protein tends to be abnormally aggregated, which resulted in the formation of basophilic cytoplasmic inclusions in neutrophil granulocytes, namely "Döhle-like" body that is regarded as a characteristic pathological change[34]. Based on our observations, NM IIA in *MYH9*^{E1384Q} aggregated into numerous and small cytoplasmic spots localized in perimembranous area, which was consistent with published clinical cases and animal experiments. However, there was no obvious oval- or spindle-shaped large inclusions detected in our experiments as previously reported[12].

The role of NM IIA in mediating actin dynamics has already been fully documented in previous investigations[23]. Our results suggested that, comparing with distinct linear membrane and diffuse peri-membrane expression in *MYH9*^{WT} group, the distribution of F-actin cytoskeleton was reorganized in *MYH9*^{E1384Q} cells, showing intermittent clumped membrane distribution without noticeable intracellular staining. Meanwhile, we also detected that the colocalization of NM IIA and F-actin was relatively decreased in mutant cells. First, we hypothesized

that the affected localization of actin may be related to the decreased amount and disturbed distribution of mutant myosin II. The "speckled" pattern of myosin IIA is consistent with the intermittent sectional distribution of membrane skeleton F-actin, suggesting that myosin IIA is very likely to be involved in restructuring the actin cytoskeleton network. Second, along with the altered biochemical properties, the ability of mutant protein that binds to actin cytoskeleton might be changed. Altered phosphorylation regulation and protein charge could remodify protein structure and conformation, which perturb filament assembly and inhibit its association with actin cytoskeleton. This finding is similar to Sung's experiments, which showed disorganization of actomyosin cytoskeleton in Sertoli cells cultured from mutant *MYH9* mice[35]. They found *MYH9*^{E1841K} mice have disorganized and thick bundles of F-actin, with decreased NM IIA and F-actin colocalization. Pertuy *et al*[33] also observed a strongly defective F-actin organization in megakaryocytes of *MYH9*$^{-/-}$ mice. Therefore, the results indicated that myosin IIA might serve as an anchor for F-actin, and normal activity of NM IIA promotes constitutive recruitment of F-actin. The disruption of F-actin distribution would potentially disturb the process of lens development and differentiation, which contributed to the onset of congenital cataract[22,36].

During the development of lens, fiber cells are differentiated from lens epithelial cells (LECs) through a morphogenesis process involving cell proliferation, migration, death and elongation Therefore, cellular functions must be vital in lens development and transparency maintenance. Previous studies have demonstrated that NM IIA could promote cancer cell growth via the p53 and MAPK/AKT signaling pathways, and regulate the epithelial-mesenchymal transition (EMT) process[36-39]. Similar to previous result, *MYH9* overexpression in our study promoted the cell proliferation, and E1384Q mutation significantly inhibit cell proliferation. The possible reason might be that NM IIA regulates proliferation-related and EMT upstream transduction pathways to regulate proliferation activity. Additionally, the actomyosin cytoskeleton, as the critical intracellular mechanosensor, is identified as the primary driver of cell migration and adhesion due to its ability to generate force and sense microenvironmental stiffness[40]. Our results revealed that WT NM IIA promoted cell migration, whereas mutants significantly reduced migration activity. Nemethova *et al*[41] revealed that actomyosin cytoskeleton contributed to the construction of contractile bundles in the filopodial lamella, initiating and promoting migration process. Moreover, we also detected increased cell apoptosis in *MYH9* E1384Q mutant cells. Similarly, Kang *et al*[42] found that primary podocytes isolated from a *MYH9* mutant mouse model showed altered structure and reorganization of actomyosin cytoskeleton along with increased motility *in vitro*. It is generally accepted that cellular apoptosis and structural injury caused by NM IIA deficiency are induced through Ca^{2+} influx and reactive oxygen species generation[43].

We also detected that E1384Q mutation resulted in the dysfunction of energy metabolism, exhibiting less number, small volume, round shape and thin crista of mitochondria. Additionally, we found several rough endoplasmic reticula and mitotic mitochondria in WT group, indicating active protein synthesis and vesicular transportation, which were not prominently found in E1384Q mutant group. The mitochondria dysfunction might exacerbate ROS generation and oxidative stress reaction, inhibiting protein synthesis and secretion and contributing to the development of congenital cataract together.

This study has some limitations. First, we applied Hek293T cell line instead of LECs for *in vitro* experiments. We did not successfully establish transfected LECs cell line in the preliminary test, and the transfection efficiency was always relatively low, which we suspected is caused by the lengthy gene segment of *MYH9*. Therefore, the logical relationship between 293T experiments and the mechanism of congenital cataract is not that direct and convinced, and we would keep trying different transfection methods to improve the expression efficiency of plasmids in LECs in the further research to provide more direct and clear evidences. However, exploring the impact of E1384Q in Hek293T cells is still of great significance for understanding the role of *MYH9* in disease development. Moreover, in the absence of *in vitro* experiments and mutant animal model, there is no histological and morphological investigations to reveal the effect of *MYH9* on the development process of lens.

In conclusion, the first mechanism research on an *MYH9* mutation with the phenotype of congenital cataract found that the missense mutation consequently resulted in decreased amount and altered subcellular distribution of NM IIA and F-actin protein, accompanied by decreased cell proliferation and migration, and induced apoptosis. The accompanied mitochondrial alteration might be involved in the development of congenital cataract.

ACKNOWLEDGEMENTS

Authors' Contributions: Yuan H and Yang JR were responsible for designing the experiments. Wang ZY was responsible for analyzing and interpreting the data. Yuan H contributed to the writing of original draft, review and editing. Huang C, Zhu L, and Li XM (the corresponding authors) took responsibility for the revising.

Data Availability: The datasets used and analyzed during the current study available from the corresponding author on reasonable request.

Foundations: Supported by Beijing Municipal Natural Science Foundation (No.7202229; No.7242168); China Primary Health Care Foundation (No.MTP2022C025).

Conflicts of Interest: Yuan H, None; **Wang ZY,** None; **Yang JR,** None; **Huang C,** None; **Zhu L,** None; **Li XM,** None.

REFERENCES

1 Pascolini D, Mariotti SP. Global estimates of visual impairment: 2010. *Br J Ophthalmol* 2012;96(5):614-618.

2 Singh R, Barker L, Chen SI, *et al*. Surgical interventions for bilateral congenital cataract in children aged two years and under. *Cochrane Database Syst Rev* 2022;9(9):CD003171.

3 Li L, Wang X, Liu CY, *et al*. Incidence rate of secondary glaucoma following congenital cataract surgery: an in-depth systematic review and meta-analysis. *Am J Ophthalmol* 2024;265:176-188.

4 Bremond-Gignac D, Daruich A, Robert MP, *et al*. Recent developments in the management of congenital cataract. *Ann Transl Med* 2020;8(22):1545.

5 Bell SJ, Oluonye N, Harding P, *et al*. Congenital cataract: a guide to genetic and clinical management. *Ther Adv Rare Dis* 2020;1:2633004020938061.

6 Hejtmancik JF. Congenital cataracts and their molecular genetics. *Semin Cell Dev Biol* 2008;19(2):134-149.

7 Yi J, Yun J, Li ZK, *et al*. Epidemiology and molecular genetics of congenital cataracts. *Int J Ophthalmol* 2011;4(4):422-432.

8 Ye HF, Zhang X, Zhao ZN, *et al*. Characterization of N6-methyladenosine long non-coding RNAs in sporadic congenital cataract and age-related cataract. *Int J Ophthalmol* 2024;17(11):1973-1986.

9 Xiao BH, Zhang SH, Ainiwaer M, *et al*. Deep learning-based assessment of missense variants in the *COG4* gene presented with bilateral congenital cataract. *BMJ Open Ophthalmol* 2025;10(1):e001906.

10 Liu YM, Ye Z, Yu HY, *et al*. A novel base substitution mutation of the CRYBA2 gene is associated with autosomal dominant congenital cataract. *Gene* 2024;927:148726.

11 Lecca M, Mauri L, Gana S, *et al*. Novel molecular, structural and clinical findings in an Italian cohort of congenital cataract. *Clin Genet* 2024;106(4):403-412.

12 Pecci A, Panza E, De Rocco D, *et al*. MYH9 related disease: four novel mutations of the tail domain of myosin-9 correlating with a mild clinical phenotype. *Eur J Haematol* 2010;84(4):291-297.

13 Pecci A, Ma XF, Savoia A, *et al*. MYH9: structure, functions and role of non-muscle myosin IIA in human disease. *Gene* 2018;664:152-167.

14 Gou ZX, Zhang DF, Cao HL, *et al*. Exploring the nexus between MYH9 and tumors: novel insights and new therapeutic opportunities. *Front Cell Dev Biol* 2024;12:1421763.

15 Feroz W, Park BS, Siripurapu M, *et al*. Non-muscle myosin II A: friend or foe in cancer *Int J Mol Sci* 2024;25(17):9435.

16 Das S, Mallick D, Sarkar S, *et al*. A brain specific alternatively spliced isoform of nonmuscle myosin IIA lacks its mechanoenzymatic activities. *J Biol Chem* 2023;299(9):105143.

17 Vicente-Manzanares M, Ma X, Adelstein RS, *et al*. Non-muscle myosin II takes centre stage in cell adhesion and migration. *Nat Rev Mol Cell Biol* 2009;10(11):778-790.

18 Weißenbruch K, Grewe J, Hippler M, *et al*. Distinct roles of nonmuscle myosin II isoforms for establishing tension and elasticity during cell morphodynamics. *eLife* 2021;10:e71888.

19 Weißenbruch K, Fladung M, Grewe J, *et al*. Nonmuscle myosin IIA dynamically guides regulatory light chain phosphorylation and assembly of nonmuscle myosin IIB. *Eur J Cell Biol* 2022;101(2): 151213.

20 Chauhan BK, Disanza A, Choi SY, *et al*. Cdc42- and IRSp53-dependent contractile filopodia tether presumptive lens and retina to coordinate epithelial invagination. *Development* 2009;136(21):3657-3667.

21 Wang ZY, Huang C, Sun YX, *et al*. Novel mutations associated with autosomal-dominant congenital cataract identified in Chinese families. *Exp Ther Med* 2019:18(4):2701-2710.

22 Houssin NS, Martin JB, Coppola V, *et al*. Formation and contraction of multicellular actomyosin cables facilitate lens placode invagination. *Dev Biol* 2020;462(1):36-49.

23 Semenova I, Burakov A, Berardone N, *et al*. Actin dynamics is essential for myosin-based transport of membrane organelles. *Curr Biol* 2008;18(20):1581-1586.

24 Zhao PX, Han HB, Wu X, *et al*. ARP2/3 regulates fatty acid synthesis by modulating lipid droplets' motility. *Int J Mol Sci* 2022;23(15):8730.

25 Barai A, Mukherjee A, Das A, *et al*. α-Actinin-4 drives invasiveness by regulating myosin IIB expression and myosin IIA localization. *J Cell Sci* 2021;134(23):jcs258581.

26 Ren X, Zhu H, Deng K, *et al*. Long noncoding RNA TPRG1-AS1 suppresses migration of vascular smooth muscle cells and attenuates atherogenesis *via* interacting with MYH9 protein. *Arterioscler Thromb Vasc Biol* 2022;42(11):1378-1397.

27 Qu JR, Qiu BJ, Zhang YX, *et al*. The tumor-enriched small molecule gambogic amide suppresses glioma by targeting WDR1-dependent cytoskeleton remodeling. *Signal Transduct Target Ther* 2023;8(1):424.

28 Zhao YL, Wilmarth PA, Cheng C, *et al*. Proteome-transcriptome analysis and proteome remodeling in mouse lens epithelium and fibers. *Exp Eye Res* 2019;179:32-46.

29 Plageman TF Jr, Chung MI, Lou M, *et al*. Pax6-dependent Shroom3 expression regulates apical constriction during lens placode invagination. *Development* 2010;137(3):405-415.

30 Vettore S, De Rocco D, Gerber B, *et al*. A G to C transversion at the last nucleotide of exon 25 of the MYH9 gene results in a missense mutation rather than in a splicing defect. *Eur J Med Genet* 2010;53(5):256-260.

31 Pecci A, Canobbio I, Balduini A, *et al*. Pathogenetic mechanisms of hematological abnormalities of patients with MYH9 mutations. *Hum Mol Genet* 2005;14(21):3169-3178.

32 Deutsch S, Rideau A, Bochaton-Piallat ML, *et al*. Asp1424Asn MYH9 mutation results in an unstable protein responsible for the phenotypes in May-Hegglin anomaly/Fechtner syndrome. *Blood* 2003;102(2): 529-534.

33 Pertuy F, Eckly A, Weber J, *et al*. Myosin IIA is critical for organelle distribution and F-actin organization in megakaryocytes and platelets. *Blood* 2014;123(8):1261-1269.

34 Savoia A, De Rocco D, Panza E, *et al*. Heavy chain myosin 9-related disease (MYH9-RD): neutrophil inclusions of myosin-9 as a pathognomonic sign of the disorder. *Thromb Haemost* 2010;103(4):826-832.

35 Sung DC, Ahmad M, Lerma Cervantes CB, *et al*. Mutations in non-muscle myosin 2A disrupt the actomyosin cytoskeleton in Sertoli cells and cause male infertility. *Dev Biol* 2021;470:49-61.

36 Wertheimer C, Liegl R, Kernt M, *et al*. EGFR-blockade with erlotinib reduces EGF and TGF-β2 expression and the actin-cytoskeleton which influences different aspects of cellular migration in lens epithelial cells. *Curr Eye Res* 2014;39(10):1000-1012.

37 Schramek D, Sendoel A, Segal JP, *et al*. Direct *in vivo* RNAi screen unveils myosin IIa as a tumor suppressor of squamous cell carcinomas. *Science* 2014;343(6168):309-313.

38 Yang B, Liu HJ, Bi YH, *et al*. MYH9 promotes cell metastasis *via* inducing angiogenesis and epithelial mesenchymal transition in esophageal squamous cell carcinoma. *Int J Med Sci* 2020;17(13):2013-2023.

39 Wang B, Qi XL, Liu J, *et al*. MYH9 promotes growth and metastasis *via* activation of MAPK/AKT signaling in colorectal cancer. *J Cancer* 2019;10(4):874-884.

40 Cagigas ML, Bryce NS, Ariotti N, *et al*. Correlative cryo-ET identifies actin/tropomyosin filaments that mediate cell-substrate adhesion in cancer cells and mechanosensitivity of cell proliferation. *Nat Mater* 2022;21(1):120-128.

41 Nemethova M, Auinger S, Small JV. Building the actin cytoskeleton: filopodia contribute to the construction of contractile bundles in the lamella. *J Cell Biol* 2008;180(6):1233-1244.

42 Kang JS, Lee SJ, Lee JH, *et al*. Angiotensin II-mediated MYH9 downregulation causes structural and functional podocyte injury in diabetic kidney disease. *Sci Rep* 2019;9:7679.

43 He W, Wang X, Zhan D, *et al*. Changes in the expression and functional activities of Myosin II isoforms in human hyperplastic prostate. *Clin Sci* (*Lond*) 2021;135(1):167-183.